ACS APPLIED MATERIALS & INTERFACES

Research Article

www.acsami.org

# Synthesis and Controllable Wettability of Micro- and Nanostructured Titanium Phosphate Thin Films Formed on Titanium Plates

Mitsunori Yada,* Yuko Inoue, Ayako Sakamoto, Toshio Torikai, and Takanori Watari

Department of Chemistry and Applied Chemistry, Faculty of Science and Engineering, Saga University, 1 Honjo, Saga 840-8502, Japan

Supporting Information

**ABSTRACT:** The hydrothermal treatment of a titanium plate in a mixed aqueous solution of hydrogen peroxide and aqueous phosphoric acid under different conditions results in the formation of various titanium phosphate thin films. The films have various crystal structures such as $Ti_2O_3(H_2PO_4)_2{\cdot}2H_2O$, $\alpha$-titanium phosphate ($Ti(HPO_4)_2{\cdot}H_2O$), $\pi$-titanium phosphate ($Ti_2O(PO_4)_2{\cdot}H_2O$), or low-crystallinity titanium phosphate and different morphologies that have not been previously reported such as nanobelts, microflowers, nanosheets, nanorods, or nanoplates. The present study also suggests the mechanisms behind the formation of these thin films. The crystal structure and morphology of the titanium phosphate thin films depend strongly on the concentration of the aqueous hydrogen peroxide solution, the amount of phosphoric acid, and the reaction temperature. In particular, hydrogen peroxide plays an important role in the formation of the titanium phosphate thin films. Moreover, controllable wettability of the titanium phosphate thin films, including superhydrophilicity and superhydrophobicity, is reported. Superhydrophobic surfaces with controllable adhesion to water droplets are obtained on $\pi$-titanium phosphate nanorod thin films modified with alkylamine molecules. The adhesion force between a water droplet and the thin film depends on the alkyl chain length of the alkylamine and the duration of ultraviolet irradiation utilized for photocatalytic degradation.

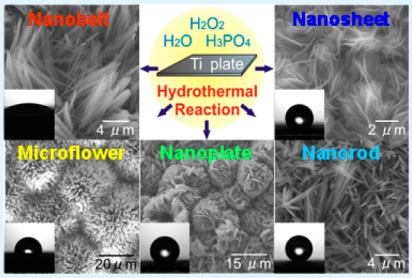


**KEYWORDS:** *hydrothermal synthesis, titanium phosphate, thin films, superhydrophobicity, superhydrophilicity*

## 1. INTRODUCTION

Various crystal structures of titanium phosphate such as $\alpha$-titanium phosphate ($Ti(HPO_4)_2{\cdot}H_2O$),[1] $\gamma$-titanium phosphate ($Ti(H_2PO_4)PO_4{\cdot}2H_2O$),[1] $\pi$-titanium phosphate ($Ti_2O(PO_4)_2{\cdot}H_2O$),[2,3] and $\rho$-titanium phosphate ($Ti_2O(PO_4)_2{\cdot}H_2O$)[2,3] have been reported, and nanostructures such as mesoporous,[4] nanotubular,[5] and hollow nanospherical[6] structures have been studied. The functions of these crystal structures and nanostructures have also been investigated. The material has been actively studied for many years for applications as a catalyst,[7,8] in lithium ion batteries,[9] in dye-sensitized solar cells,[10,11] as a selective absorbent of useful and hazardous substances,[12−14] for adhesion and release of drugs,[15] and as a label for ultrasensitive electrochemical detection of human interleukin-6.[6] These studies have primarily focused on titanium phosphate particles; titanium phosphate thin films have not yet been thoroughly examined, except for several studies using the layer-by-layer adsorption and reaction method[16,17] or the electrochemical deposition method.[18]

Recently, as research on nanoparticles has progressed, it has become clear that to maximize and make effective use of the chemical and physical characteristics of nanoparticles it is important to fabricate thin films composed of these nanoparticles. Of particular interest are nanostructured inorganic compound thin film/metal composites that are obtained by forming a nanostructured inorganic compound thin film on a metal surface using the metal as an inorganic compound source. These composites have been reported to be excellent materials as good adherence is realized between the metal and the thin film since the thin film grows directly on the metal surface. They are also exceptional materials because of their mechanical properties and conductivity, which are peculiar to the metal, as well as their chemical and physical properties arising from the nanostructured inorganic compound thin film. The formation of a nanostructured titanium compound thin film on a titanium surface and its resulting applications have been reported before. For example, titanium dioxide nanotube thin film/titanium composites[19,20] can be used as materials for preparing photocatalyst, solar cells, electrochromic devices, medical implants, and field emission devices. Silver nanoparticle/silver titanate nanotube thin film/titanium composites can be used as implant materials with excellent apatite-forming and antibacterial abilities.[21,22]

The synthesis of a titanium phosphate thin film on a titanium surface has been reported in two studies. In both studies,[23,24] use of an aqueous phosphoric acid solution for the hydrothermal reaction of titanium led to the formation of a thin film of $\pi$-titanium phosphate nanorods on the titanium surface. Park et al.[24] reported that the thin film exhibited excellent osteoconductivity. Therefore, the titanium phosphate thin

Received: February 16, 2014
Accepted: April 8, 2014
Published: April 8, 2014

  

**Table 1. Relationship between Synthesis Conditions and Thin Films**

| | synthesis condition | | | | | product | |
|---|---|---|---|---|---|---|---|
| sample no. | 30 wt % $H_2O_2$ aq./mL | $H_2O$/mL | 85 wt % $H_3PO_4$ aq./g | temperature/°C | reaction time/h | crystal structure | morphology |
| **1** | 9.2 | 0 | 0.5 | 120 | 24 | $Ti_2O_3(H_2PO_4)_2{\cdot}2H_2O$ | nanobelt thin film |
| **2** | 0 | 9.2 | 0.5 | 120 | 24 | $TiH_2$ | smooth surface |
| **3** | 2.3 | 6.9 | 0.5 | 120 | 24 | $Ti_2O_3(H_2PO_4)_2{\cdot}2H_2O$ | microflower thin film |
| **4** | 9.2 | 0 | 0 | 120 | 24 | $TiO_2$ | nanorod thin film |
| **5** | 9.2 | 0 | 5.0 | 120 | 24 | $Ti(HPO_4)_2{\cdot}H_2O$ | nanoplate thin film |
| **6** | 9.2 | 0 | 0.5 | 80 | 24 | low crystallinity | nanosheet thin film |
| **7** | 9.2 | 0 | 0.5 | 160 | 24 | $Ti_2O(PO_4)_2{\cdot}H_2O$ | nanorod thin film |

films with various crystal structures and nanomorphologies formed on titanium surfaces by employing new synthetic methods will be useful as materials for medical implants, solar cells, catalysts, and adsorbents. Unlike the previous two studies, the present study considers the synthesis of a titanium phosphate thin film on a titanium surface through hydrothermal treatment of a titanium plate in a mixed aqueous solution of hydrogen peroxide and phosphoric acid. Carrying out the hydrothermal treatment under different conditions results in titanium phosphate thin films with different crystal structures such as $Ti_2O_3(H_2PO_4)_2{\cdot}2H_2O$, $\alpha$-titanium phosphate, $\pi$-titanium phosphate, or low-crystallinity titanium phosphate and various morphologies that have not been previously reported, such as nanobelts, microflowers, nanosheets, nanorods, or nanoplates. The present study also suggests the mechanisms behind the formation of these thin films.

Recently, the control of materials' wettability has attracted significant attention because of the promising applications such as in preparation of self-cleaning materials, corrosion resistance, fluidic drag reduction, and oil–water separation.[25−31] In general, the surface wettability of a solid depends on its surface free energy and the surface micro- and/or nanostructures of the solid.[26,27] From the Cassie–Baxter equation,[32] it is well known that nanostructured thin films whose surfaces are modified with organic molecules with low surface free energies exhibit superhydrophobic properties.[26,27] Moreover, superhydrophobic thin films with strong adhesion to liquid droplets have increasingly attracted attention owing to their potential applications in liquid droplet transportation[33,34] and sample assays.[33] Only a few studies have however reported the successful control of the adhesion force of these films while maintaining their superhydrophobicity.[33−37] The wettability of titanium phosphate thin films has also not been studied so far. In the present study, controllable wettability of titanium phosphate thin films including superhydrophilicity and superhydrophobicity with controllable adhesion to water droplets is reported.

## 2. EXPERIMENTAL SECTION

**Synthesis.** After a titanium plate (20 × 20 × 0.5 mm, Nilaco Corporation) was polished with a sandpaper and then soaked in 10 mL of a 2 mol/L aqueous hydrogen fluoride solution for 10 min to remove the oxidized layer on its surface, it was repeatedly washed with distilled water. An ultrathin oxidized layer (passivation film) reforms on the titanium plate surface by washing the plate with water after treating it with the hydrogen fluoride solution, but this operation was conducted to create a nearly equal surface condition for each of the experiments. The plate was then hydrothermally reacted to form a titanium phosphate thin film on the plate in a mixture of 30 wt % aqueous hydrogen peroxide solution (Sigma-Aldrich Co. LLC) and 85 wt % aqueous phosphoric acid solution (Wako Pure Chemical Industries, Ltd.) in a Teflon container. The hydrothermal reactions were performed in different conditions as summarized in Table 1. After the reaction, the plate was repeatedly washed under a strong stream of distilled water to prevent titanium phosphate particles which are generated and suspended during the synthesis of the thin film from adsorbing onto the thin-film surface, but detachment of the thin film from the plate was not verified.

**Characterization.** Particles formed in the solution during the reaction were deposited on the titanium plate after the reaction, preventing us from correctly evaluating the morphology of the titanium phosphate growing on the titanium plate. Therefore, the back surface of the titanium plate, on which no particles were deposited, was evaluated in detail using scanning electron microscopy (SEM), transmission electron microscopy (TEM), energy-dispersive X-ray microanalysis (EDX), X-ray diffraction (XRD), and Fourier transform infrared absorption analysis (FT-IR). TEM was carried out using a JEOL JEM-1210 instrument. SEM was performed using a Hitachi S-3000N. EDX was conducted with an EDAX Genesis 2000 instrument. The molar ratio of P/Ti determined by EDX analysis is the average molar ratio from three measurement locations. XRD measurements were performed using a Shimadzu XRD-6100 instrument with Cu K$\alpha$ radiation. The FT-IR spectrum was measured using a Nippon Bunko FT/IR-300 apparatus. In many cases, the wettability was evaluated by measuring the contact angle with a contact angle meter (DropMaster 500 and DMe-201; Kyowa Interface Science Co. Ltd.) after 2 $\mu$L of distilled water was dropped onto the thin film. However, 4 $\mu$L and 6 $\mu$L water droplets were also used, when the 2 $\mu$L water droplet was not adsorbed by the film because of its enhanced superhydrophobicity. In this procedure, the contact angle was measured following the $\theta/2$ method using an image of the droplet obtained 1 s after it was dropped. The sliding angle was measured by tilting the plate with the 10 $\mu$L water droplet on it.

**Photocatalytic Degradation.** A 27 W black light source (maximum wavelength, $\lambda$ = 368 nm) was utilized as the ultraviolet light source, and the thin film was subjected to ultraviolet irradiation by using the black light source that was positioned at a distance of 5 cm. A 2 $\mu$L water droplet was used to determine the contact angle of the nanorod thin film treated with the dodecylamine solution, and the measurement was performed at three or four locations. However, a 4 $\mu$L water droplet was used on the nanorod thin film treated with the octadecylamine solution since the 2 $\mu$L water droplet was not adsorbed by the film even after 12 h of irradiation.

## 3. RESULTS AND DISCUSSION

**3.1. Synthesis and Formation Mechanism of $Ti_2O_3(H_2PO_4)_2{\cdot}2H_2O$ Nanobelt and Microflower Thin Films.** When the reaction was carried out between using 9.2 mL of aqueous hydrogen peroxide solution and 0.5 g of aqueous phosphoric acid solution at 120 °C for 24 h, a thin film composed of nanobelts approximately 30–270 nm wide and several micrometers long was evenly formed on the titanium plate, as shown in Figures 1a and 1b. The nanobelt thin film is termed **1** in Table 1 and the figures. The TEM image (Figure 1c) confirms that the particles in the thin film were thin nanobelts. The film thickness is approximately 8 $\mu$m. The XRD

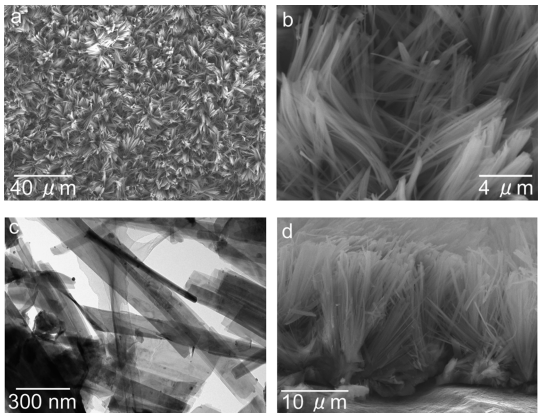


**Figure 1.** SEM images (a, b, and d) and a TEM image (c) of **1**.

pattern shown in Figure 2a exhibits diffraction peaks attributed to $Ti_2O_3(H_2PO_4)_2{\cdot}2H_2O$[38,39] in addition to the peak attributed to titanium. Therefore, the nanobelts are composed of $Ti_2O_3(H_2PO_4)_2{\cdot}2H_2O$. EDX analysis revealed that the molar ratio of P/Ti was 1.03 (Figure S1a in the Supporting Information). This value is close to the value of P/Ti = 1 estimated from the XRD measurement, i.e., based on the composition of $Ti_2O_3(H_2PO_4)_2{\cdot}2H_2O$. Kőrösi et al.[15] reported rectangular nanoparticles with sizes of (15 ± 3) nm × (20−150) nm as the morphology of $Ti_2O_3(H_2PO_4)_2{\cdot}2H_2O$. In the present study, it is assumed that these rectangular nanoparticles grew extensively in the major axis direction to form the nanobelts. The film thickness increased with increasing reaction time. Figure 1d shows an SEM image of a thin-film cross section obtained after a reaction time of 72 h. The film thickness is approximately 20 μm, and a phase composed of nanobelts is observed from the thin-film surface to a depth of approximately 18 μm. A dense phase of approximately 2 μm in thickness is present in the lower part of the film.

The effect of hydrogen peroxide on the thin-film formation was investigated by fixing the reaction temperature, reaction period, and the amount of aqueous phosphoric acid solution at 120 °C, 24 h, and 0.5 g, respectively, and varying the amount of aqueous hydrogen peroxide solution. When 9.2 mL of water was used instead of the aqueous hydrogen peroxide solution, no thin film was formed, as shown in Figure 3a, but $TiH_2$ was observed in the XRD pattern (Figure 2b). The obtained product is referred to as **2** in Table 1 and the figures. Therefore, hydrogen peroxide is important for thin-film formation. The ultrathin oxidized layer (passivation film) formed on the titanium plate surface dissolves to form a titanium surface in the reaction solution. Hydrogen peroxide is considered to play two major roles. The first role is oxidization: hydrogen peroxide acts as an oxidizer in an acid solution, following the reaction formula

$$H_2O_2 + 2H^+ + 2e^- \rightarrow 2H_2O$$

Hydrogen peroxide thus facilitates the generation of $Ti^{4+}$ from the titanium surface as shown in the following formula

$$Ti + 2H_2O_2 + 4H^+ \rightarrow Ti^{4+} + 4H_2O$$

$$(H_2O_2 + 2H^+ + 2e^- \rightarrow 2H_2O,\ Ti \rightarrow Ti^{4+} + 4e^-)$$

$Ti^{4+}$ is also generated from reactions with $H^+$ and dissolved oxygen in the solution, following the reaction formulas

$$Ti + 4H^+ \rightarrow Ti^{4+} + H_2$$

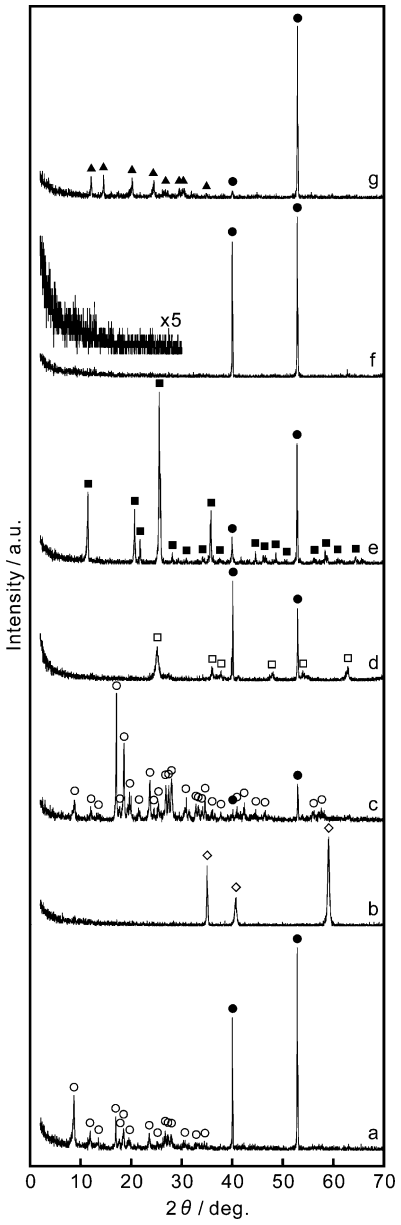


**Figure 2.** XRD patterns of (a) **1**, (b) **2**, (c) **3**, (d) **4**, (e) **5**, (f) **6**, and (g) **7**. Peak assignment: ●, Ti; ○, $Ti_2O_3(H_2PO_4)_2{\cdot}2H_2O$; ◇, $TiH_2$; □, $TiO_2$ (anatase); ■, $Ti(HPO_4)_2{\cdot}H_2O$; ▲, $Ti_2O(PO_4)_2{\cdot}H_2O$.

$$Ti + O_2 + 2H_2O \rightarrow Ti^{4+} + 4OH^-$$

However, hydrogen peroxide has the greatest effect on facilitating $Ti^{4+}$ generation. Immediately after elution from Ti to the reaction solution, $Ti^{4+}$ reacts with $H_2O_2$. When pH < 1, $Ti^{4+}$ is known to form complexes such as $Ti(O_2)(OH)_{n-2}^{(4-n)+}$.[40] When pH > 1, $Ti^{4+}$ is known to form binuclear complexes such as $Ti_2O_5(OH)_x^{(2-x)}$ ($x$ = 1−6).[40] Thus, the second role of hydrogen peroxide is to form chemical species that possess Ti−O bonds. When these chemical species react with phosphate or hydrogen phosphate ions, amorphous or low-crystallinity titanium phosphate is first deposited on the titanium plate to form a dense phase. High-crystallinity titanium phosphate, which is the most stable phase under certain synthetic conditions, then grows from the surface of the dense phase to form a nanostructured titanium phosphate thin film possessing a crystal structure and morphology specific to the


dx.doi.org/10.1021/am500974v | ACS Appl. Mater. Interfaces 2014, 6, 7695−7704

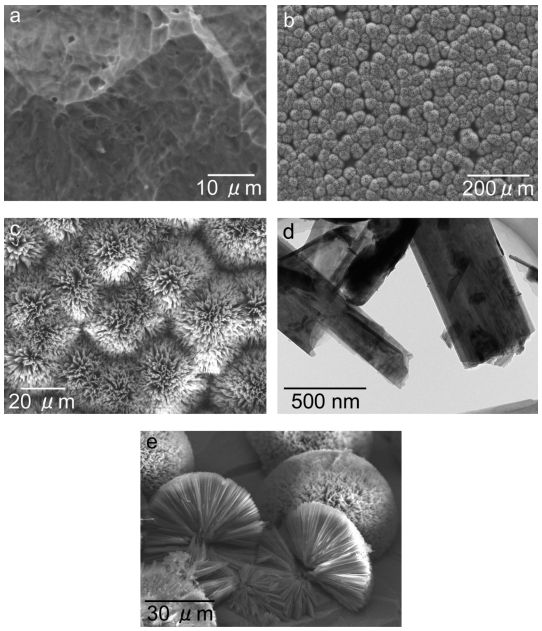


**Figure 3.** Effect of aqueous hydrogen peroxide solution on thin-film morphology: SEM images (a, b, c, and e) and a TEM image (d) of (a) **2** and (b–e) **3**.

synthetic conditions. This phenomenon, in which a specific nanostructured thin film is formed through the formation of a dense phase on a metal surface, was previously observed during the formation of a sodium titanate thin film on the surface of a titanium plate.[41,42] Another mechanism underlying the titanium phosphate thin-film formation may involve a direct reaction of $Ti^{4+}$, $H_2O_2$, and phosphate or hydrogen phosphate ions to form polynuclear complexes with complicated structures and compositions containing Ti, P, O, and H. Through a polycondensation reaction, these polynuclear complexes are redeposited on the titanium plate as crystalline titanium phosphate to form a titanium phosphate thin film.

When a mixture of 2.3 mL of aqueous hydrogen peroxide solution and 6.9 mL of water was used instead of the 9.2 mL of aqueous hydrogen peroxide solution, a thin film composed of hemispheric and flowerlike aggregates approximately 30–40 $\mu$m in diameter was formed (Figures 3b and 3c). The thin film composed of flowerlike aggregates is referred to as **3** in Table 1 and the figures. Interestingly, SEM images (Figures 3c and 3e) and a TEM image (Figure 3d) reveal that the nanoplate-shaped particles are hundreds of nanometers (approximately 400–700 nm) wide and approximately 28 $\mu$m long and grow radially to form the flowerlike aggregates. Figure 3e indicates broken flowerlike aggregates and is particularly important for understanding the detailed structure of the thin film and for discussing its process for the formation of the thin film. The XRD pattern (Figure 2c) indicates that this thin film is composed of $Ti_2O_3(H_2PO_4)_2{\cdot}2H_2O$, as is the nanobelt thin film. However, a comparison of the diffraction peaks in Figures 2a and 2c reveals that the intensity ratio of the diffraction peaks is different overall, particularly near $2\theta = 10°$. The intensity of the diffraction peak near $2\theta = 10°$ is markedly lower for this thin film than for the nanobelt thin film. In a crystal of nanobelt- or nanoplate-shaped $Ti_2O_3(H_2PO_4)_2{\cdot}2H_2O$, titanium phosphate layers are stacked parallel to the long axis of the crystal to form a crystal with a layered structure. In the microflower thin film, since the crystal with the layered structure is tilted or perpendicular to the metal titanium plate in many cases, the intensity of the diffraction peak near $2\theta = 10°$ corresponding to the interlayer distance of the layered structure is lower. The molar ratio of P/Ti obtained from the EDX analysis was 0.96 (Figure S1b in the Supporting Information). This value is similar to the value of P/Ti = 1 estimated from the composition of $Ti_2O_3(H_2PO_4)_2{\cdot}2H_2O$. These results suggest the following process for the formation of the thin film composed of flowerlike aggregates: (1) When the amount of hydrogen peroxide in the reaction solution decreases, the number of titanium phosphate nuclei formed on the titanium plate also decreases markedly. (2) Then, crystals composed of titanium phosphate ($Ti_2O_3(H_2PO_4)_2{\cdot}2H_2O$) slowly grow radially from a small number of formed nuclei. (3) Finally, the thin film composed of flowerlike aggregates forms. Because the crystals grow slowly, they have high crystallinity and form nanoplate-shaped particles with high aspect ratios instead of nanobelts.

**3.2. Synthesis of $\alpha$-Titanium Phosphate Nanoplate Thin Film.** The effect of phosphoric acid on the formation of thin films was investigated by setting the reaction temperature and the amount of aqueous hydrogen peroxide solution to 120 °C and 9.2 mL, respectively, and varying the amount of aqueous phosphoric acid solution. When the amount of aqueous phosphoric acid solution was 0 g, a thin film composed of nanorods tens of nanometers wide and approximately 2 $\mu$m long with a thickness of approximately 2 $\mu$m was formed (Figure 4a). The nanorod thin film is referred

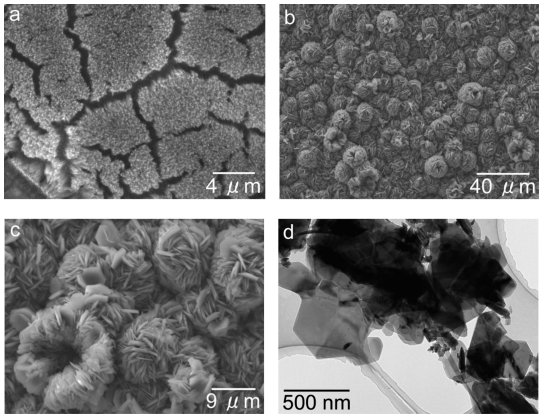


**Figure 4.** Effect of aqueous phosphoric acid solution on thin-film morphology: SEM images (a–c) and a TEM image (d) of (a) **4** and (b–d) **5**.

to as **4** in Table 1 and the figures. The XRD pattern (Figure 2d) reveals that this nanorod thin film was composed of anatase-type $TiO_2$, in agreement with the results of Wu et al.,[43] who performed a hydrothermal treatment on a titanium plate in an aqueous hydrogen peroxide solution and formed an anatase-type $TiO_2$ nanorod thin film on the plate surface. When the amount of aqueous phosphoric acid solution was 5 g, hexagonal nanoplates with sizes of several micrometers were vertically aggregated to form a thin film, as shown in Figures 4b–d. The nanoplate thin film is indicated by **5** in Table 1 and the figures. As shown in Figure 4c and Figure S2 in the Supporting Information, mainly hexagonal nanoplates aggregated hemispherically to form dense structures, but some hexagonal nanoplates also aggregated hemispherically to form hollow structures. The cross section of the formed thin film had a

thickness of approximately 8 $\mu$m. The XRD pattern reveals that the thin-film crystal structure is $\alpha$-titanium phosphate, Ti-$(HPO_4)_2{\cdot}H_2O$ (Figure 2e). The molar ratio of P/Ti obtained from the EDX analysis was 1.96 (Figure S1c in the Supporting Information). This value is similar to the value of P/Ti = 2 estimated from the composition of $\alpha$-titanium phosphate. The $H_2O_2$ concentration decreased as the amount or concentration of phosphoric acid increased. Consequently, the formation of Ti−O bonds was inhibited, and $\alpha$-titanium phosphate was generated.

**3.3. Synthesis of Low-Crystallinity Titanium Phosphate Nanosheet and $\pi$-Titanium Phosphate Nanorod Thin Films.** The effect of the reaction temperature on the formation of a thin film was investigated by fixing the amounts of aqueous hydrogen peroxide solution and aqueous phosphoric acid solution at 9.2 mL and 0.5 g, respectively, and varying the reaction temperature. When the reaction temperature was 80 °C, a thin film composed of nanosheets with sizes between hundreds of nanometers and 2 $\mu$m was formed with a film thickness of approximately 3 $\mu$m, as shown in Figure 5a−c.

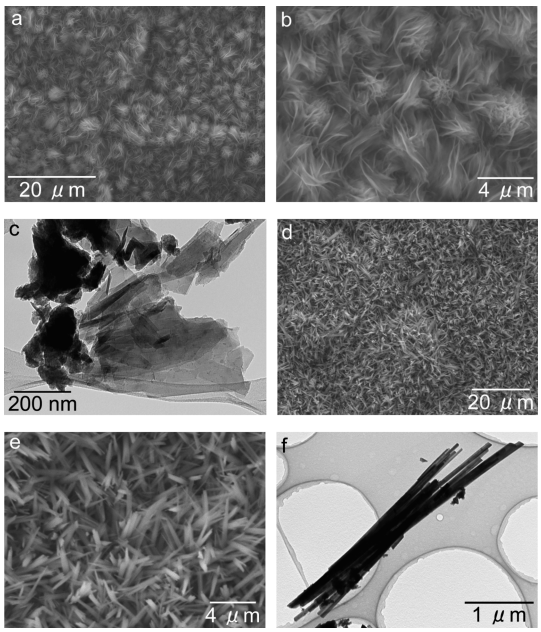


**Figure 5.** Effect of reaction temperature on thin-film morphology: SEM images (a, b, d, and e) and TEM images (c and f) of (a−c) **6** and (d−f) 7.

The nanosheet thin film is termed **6** in Table 1 and the figures. The molar ratio of P/Ti obtained from the EDX measurements was 0.49 (Figure S1d in the Supporting Information); i.e., the amount of P was quite small. The reason for this small molar ratio is probably the thinness of the titanium phosphate thin film, which allowed the Ti in the titanium plate below it to be detected in the EDX measurement. The XRD pattern in Figure 2f shows only a broad peak with a low intensity near $2\theta$ = 10° for the thin film formed at 80 °C. This indicates the formation of a low-crystallinity titanium phosphate thin film with a layered structure. Thin-film XRD measurement of the thin film was also conducted to investigate its crystal structure in further detail. The result shows a sharp diffraction peak at $2\theta$ = 8.7°, while broad and low-intensity diffraction peaks emerge at around $2\theta$ = 12°, 18°, and 28° (Figure S3 in the Supporting Information). The locations of the diffraction peaks are similar to those observed in the case of $Ti_2O_3(H_2PO_4)_2{\cdot}2H_2O$, indicating that the thin film was derived from $Ti_2O_3(H_2PO_4)_2{\cdot}2H_2O$ with low crystallinity. When the reaction temperature was 160 °C, a thin film composed of nanorods that were approximately 30−150 nm in width and several micrometers in length was formed, as shown in Figure 5d−f. The nanorod thin film is referred to as **7** in Table 1 and the figures. The cross section of this thin film reveals a thickness of approximately 7 $\mu$m. The XRD pattern indicates that the nanorod thin-film crystal structure was attributable to $\pi$-titanium phosphate, $Ti_2O(PO_4)_2{\cdot}H_2O$ (Figure 2g). The molar ratio of P/Ti obtained from the EDX analysis was 0.77 (Figure S1e in the Supporting Information), which is smaller than the value of P/Ti = 1 estimated based on the composition of $Ti_2O(PO_4)_2{\cdot}H_2O$. The reason for this small molar ratio is considered to be the many gaps in the $\pi$-titanium phosphate thin film that allow the Ti in the titanium plate below the thin film to be detected. As mentioned above, two studies have reported on the formation of a $\pi$-titanium phosphate thin film on a titanium surface. Lu et al.[23] obtained a thin film composed of $\pi$-titanium phosphate nanorods by performing a hydrothermal treatment of a titanium plate in a phosphoric acid solution at 250 °C. Park et al.[24] also obtained a $\pi$-titanium phosphate thin film that was approximately 5 $\mu$m thick and had needle-like surface microstructures by performing a hydrothermal treatment of the titanium plate in a phosphoric acid solution at 180 °C. The morphology of the $\pi$-titanium phosphate nanorod thin film obtained in this study (Figures 5d−f) is finer and more homogeneous than those of the $\pi$-titanium phosphate thin films reported in the previous two studies.[23,24] In addition, the temperature used to obtain the $\pi$-titanium phosphate thin film in the present study was lower than that used in the previous two studies. These differences in the morphology and synthetic conditions are likely due to the different mechanisms behind the formation of the $\pi$-titanium phosphate thin film in the presence of hydrogen peroxide.

**3.4. Wettability of Titanium Phosphate Thin Films.** In the present study, the wettability of the $\pi$-titanium phosphate ($Ti_2O(PO_4)_2{\cdot}2H_2O$) nanorod thin film, which possesses the finest nanostructure studied here, was investigated in detail. The contact angle of the titanium plate (the raw material) was 83° (Figure 6a), whereas that of the nanorod thin film was 0° (Figure 6b). Therefore, the hydrophilicity greatly increased after the formation of the nanorod thin film; i.e., superhydrophilicity of the surface was obtained. The reason for this superhydrophilicity is probably that $\pi$-titanium phosphate has a highly hydrophilic surface (high surface free energy) and the $\pi$-titanium phosphate nanorod thin film has a large specific surface area.

Attempts were also made to lower the surface free energy of the thin film by performing chemical modification through adsorption of surfactants on the $\pi$-titanium phosphate nanorod surface. A $\pi$-titanium phosphate nanorod thin film was soaked in 20 mL of 2-propanol solution containing 0.1 mol/L *n*-dodecylamine hydrochloride at 60 °C for 5 h and was then repeatedly washed with 2-propanol to remove excess surfactants. SEM observation confirmed that there were no changes in the morphology of the nanorod thin film before or after the surface modification with the *n*-dodecylamine hydrochloride solution. The use of *n*-dodecylamine hydrochloride resulted in a change in the contact angle of the thin film to 151° (Figure 6c); i.e., a superhydrophobic surface was obtained. Therefore, surface modification with *n*-dodecylamine hydrochloride is extremely useful for controlling the wettability.

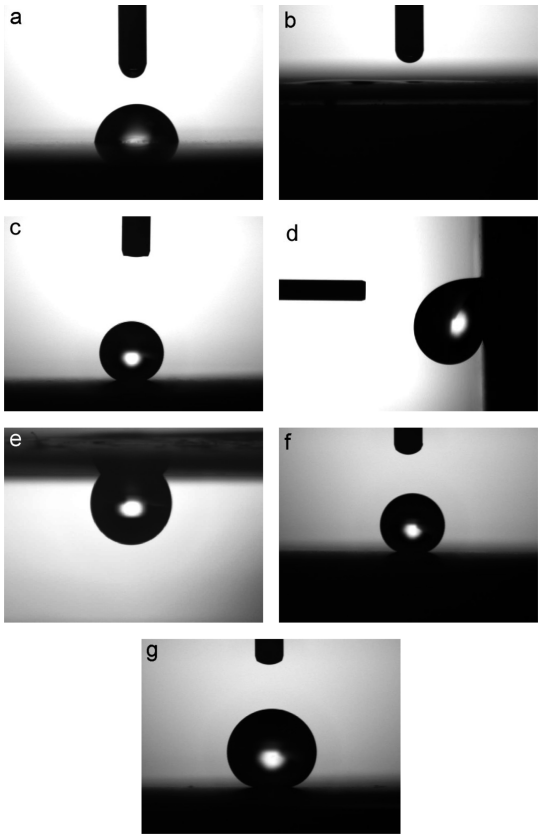


**Figure 6.** Photographs of water droplets on various samples taken with a digital camera: (a) titanium plate, (b) 7, (c) 7 treated with 0.1 mol/L *n*-dodecylamine hydrochloride solution, (d) 7 treated with 0.1 mol/L *n*-dodecylamine hydrochloride solution and then rotated 90°, (e) 7 treated with 0.1 mol/L *n*-dodecylamine hydrochloride solution and then rotated 180°, (f) 7 treated with 0.1 mol/L dodecylamine solution, and (g) 7 treated with 0.1 mol/L octadecylamine solution.

When the $\pi$-titanium phosphate nanorod thin film was soaked in 20 mL of a 0.01 mol/L aqueous methylene blue solution at 40 °C for 24 h and repeatedly washed with distilled water, the color of the nanorod thin film changed to blue, as shown in Figure S4 in the Supporting Information (i.e., positively charged methylene blue ions were adsorbed onto the $\pi$-titanium phosphate nanorod surface). Therefore, *n*-dodecylamine hydrochloride is also considered to be electrostatically adsorbed onto the $\pi$-titanium phosphate nanorod surface as $CH_3(CH_2)_{11}NH_3^+$. The FT-IR spectrum of the $\pi$-titanium phosphate nanorod thin film treated with the *n*-dodecylamine hydrochloride solution also exhibited adsorption bands at 2927 and 2857 $cm^{-1}$ due to the $-CH_2-$ group of *n*-dodecylamine, as shown in Figure S5 in the Supporting Information. Surprisingly, when the nanorod thin film was rotated 90° (Figure 6d) and 180° (Figure 6e) with a 10 $\mu$L water droplet on it, the droplet continued to adhere to the nanorod thin-film surface while retaining its almost globular shape. This indicates that an extremely large energy contributes to the adhesion. Next, a $\pi$-titanium phosphate nanorod thin film was soaked in 20 mL of ethanol solution containing 0.1 mol/L octylamine, dodecylamine, or octadecylamine at 60 °C for 5 h and was then repeatedly washed with water to remove excess surfactants. SEM observation confirmed that there were no changes in the morphology of the nanorod thin film before or after the surface modification by these three types of alkylamine solutions. The uses of octylamine and dodecylamine for surface modification also resulted in changing the contact angle of the thin film to 148° (Figure S6 in the Supporting Information) and 153° (Figure 6f), respectively, along with strong adhesion similar to that of the *n*-dodecylamine hydrochloride system. The use of octadecylamine for surface modification also resulted in a change in the contact angle of the thin film to 155° (Figure 6g), indicating the expression of superhydrophobicity. However, as soon as the thin film with the droplet was tilted beyond 11°, the droplet readily rolled off its surface because of the superhydrophobicity and decreased adhesive force. These results indicate that adhesion force between a thin film and a water droplet can be controlled by modifying the alkyl chain length of the surfactant used to modify the surface.

The expression of superhydrophobicity along with strong adhesion has been attributed to two mechanisms. The first mechanism involves the formation of a hierarchical micro- and nanostructure,[44] a well-designed nanoporous structure,[35] and a pillar array with a microsized period[34] on the thin-film surface consisting of substances with low surface energies. The second mechanism involves the formation of a rough surface structure on the micro- and/or nanoscale that possesses both superhydrophilic domains and superhydrophobic domains at the nanoscale.[33,36,37] The superhydrophobicity with strong adhesion observed in this study is considered to be attributable to the latter mechanism. When the nanorod thin film was observed in detail using SEM (Figures 5d and 5e), several nanorods appeared to aggregate to form a bundle, and many bundles grew perpendicular to the surface of the Ti plate. The formation of this hierarchical micro- and nanostructure and subsequent surface modification with surfactants with low surface energies are considered to result in the superhydrophobicity of the surface. When the nanorod thin film was treated with the *n*-dodecylamine hydrochloride solution or the dodecylamine solution, the surface modification of the film may have been incomplete. Thus, domains on which dodecylamine was adsorbed exhibited hydrophobicity, and those on which dodecylamine was not adsorbed and titanium phosphate was exposed exhibited hydrophilicity, as shown in Figure 7. Therefore, the possibility remained that since domains

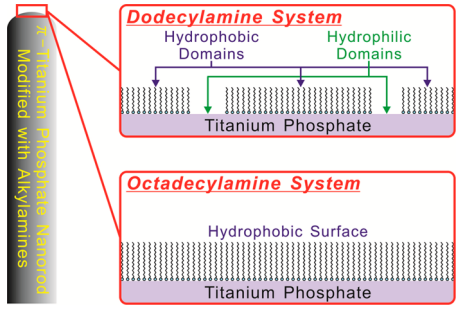


**Figure 7.** Schematic representation of 7 treated with the alkylamine solutions.

with hydrophobicity and hydrophilicity were mixed in the nanorod thin film superhydrophobicity and strong adhesion of the film to a water droplet can be coexpressed. On the other hand, when the film was treated with the octadecylamine solution, the film surface was almost completely covered with octadecylamine molecules because of their longer alkyl chain length as compared to dodecylamine, as shown in Figure 7. Therefore, domains with hydrophobicity were predominantly

formed, and those with hydrophilicity almost disappeared, resulting in the expression of superhydrophobicity along with weak adhesion to the water droplet. When the alkyl chain length of the alkylamine was longer, denser and more stable surface modification with alkylamine molecules was achieved because of stronger London dispersive forces which contributed to form hydrophobic domains. Further, when the alkyl chain length was shorter, a larger amount of alkylamine was desorbed upon washing with 2-propanol or water, resulting in the formation of hydrophilic domains. These considerations can be well applied to the result of the nanorod thin film treated with the octylamine solution. The procedure proposed in this study for controlling the wettability and adhesion of thin films to water droplets by utilizing the difference in the alkyl chain length is much simpler than previously reported procedures that use organic molecules with complicated structures and compositions such as poly(methacrylate), amphiphilic polyurethane, and hydrophobic fluorinated polyurethane;[33] hydrophobic 1*H*,1*H*,2*H*,2*H*-perfluorooctyltriethoxysilane and nitrocellulose;[36] and poly(styrene sulfonic acid) sodium salt and polydimethylsiloxane or polytetrafluoroethylene.[37]

To examine whether the schematic representation shown in Figure 7 is accurate, changes in the contact angle due to the photocatalytic degradation of alkylamines were investigated by subjecting the nanorod thin films treated with the alkylamine solutions to ultraviolet irradiation. Figure 8 shows changes in the contact angle with the ultraviolet irradiation time. When the nanorod thin film treated with the dodecylamine solution was subjected to ultraviolet irradiation (Figure 8a), the contact angle was observed to be about 150° after 20 h of irradiation. However, after 20 h of irradiation, the contact angle started to decrease and became more dispersed with increasing irradiation time. In particular, the contact angle decreased rapidly after 41 h of irradiation and became 90° or less. Highly hydrophilic areas with a contact angle of about 10° started to emerge as well after 42 h of irradiation. On the other hand, as shown in Figure 8b, superhydrophobic surfaces were maintained on the nanorod thin film treated by the octadecylamine solution even after 36 h of irradiation because the contact angle on the film was greater than or equal to 150° in most areas. After 37 h of irradiation, the contact angle started to decrease and became more dispersed with increasing irradiation time. Particularly, after 96 h of irradiation, the contact angle decreased rapidly and became 90° or less together with a relatively high contact angle of about 130−140°. Highly hydrophilic areas with a contact angle of about 20° also began to emerge after 120 h of irradiation. These results indicate that it is possible to control the contact angle of a thin film by subjecting it to ultraviolet irradiation. Moreover, changes in the contact angle due to differences in the alkyl chain length for alkylamines indicate the accuracy of the model shown in Figure 7. Uetsuka et al.[45] reported that if partial degradation of trimethylacetic acid (TMA) ions causes a gap of a few nanometers along the diameter when titanium dioxide with TMA tightly adsorbed on its surface is subjected to ultraviolet irradiation then TMA present around the gap becomes degraded as a result of chain reactions. These phenomena then lead to a significant acceleration of the photocatalytic degradation of TMA. Rapid decreases in the contact angle were observed in this study with increasing duration of ultraviolet irradiation, suggesting that photocatalytic degradation similar to that in the case of titanium dioxide occurred. Therefore, as shown in Figure 7, a long period of time was required until the degradation of

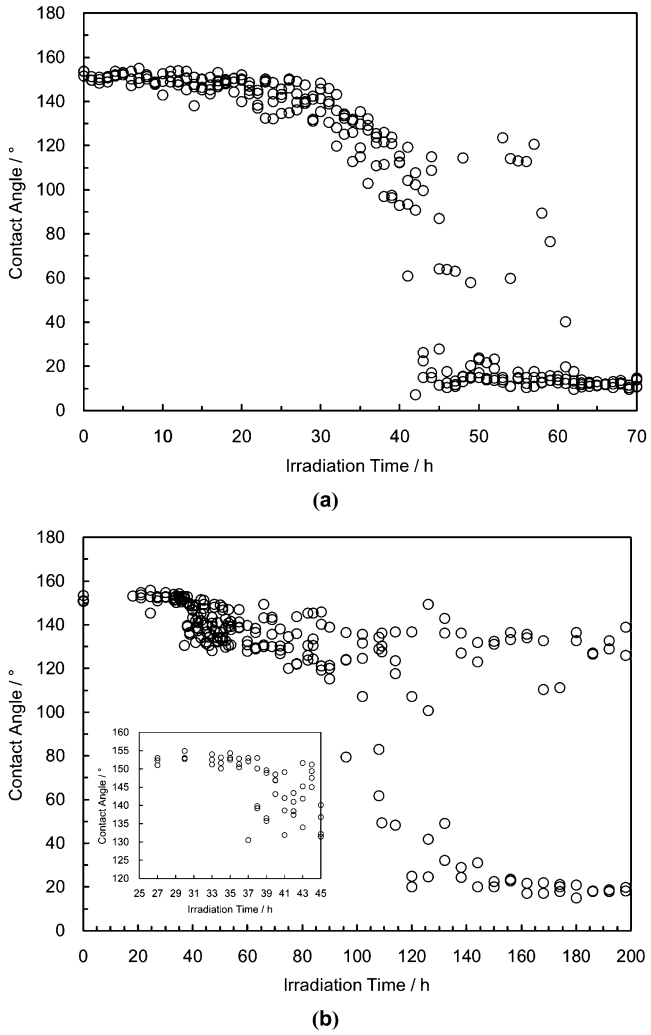


**Figure 8.** Changes in the contact angle of 7 treated with the dodecylamine (a) and the octadecylamine (b) solutions with the ultraviolet irradiation time.

octadecylamine led to gap formation on the thin film treated with the octadecylamine solution; few gaps were formed prior to the ultraviolet irradiation owing to the tight adsorption of octadecylamine on the titanium phosphate surface. This is believed to be the reason for the longer time required for the rapid decrease in the contact angle. Further, this is in contrast to rapid decreases in the contact angle in a short period of time caused by the rapid degradation of dodecylamines via chain reactions around the gaps on the nanorod thin film treated with the dodecylamine solution, with gaps formed already in the dodecylamine adsorption layer prior to the ultraviolet irradiation, as shown in Figure 7. Additionally, a more interesting feature is that when the film was tilted a water droplet rolled down on the nanorod thin film after the film was treated with the octadecylamine solution following up to 33 h of ultraviolet irradiation. However, areas on which the water droplet remained adsorbed as well as those on which it rolled down upon tilting of the film were simultaneously observed on the same thin film after 34 and 35 h of irradiation, respectively. After 36 h of irradiation, the water droplet remained adsorbed on the thin film even when the film was rotated by 90° and 180°; despite this, the film showed a superhydrophobic surface for which the contact angle was greater than or equal to 150°.


dx.doi.org/10.1021/am500974v | ACS Appl. Mater. Interfaces 2014, 6, 7695−7704

These findings suggest that adhesion forces are applied on a water droplet on the thin film because 34 h of ultraviolet irradiation degrades the octadecylamine adsorption layer and then exposed the surface of a certain area of titanium phosphate, as evidenced in the nanorod thin film treated with the dodecylamine solution. These results indicate that adhesion forces on a water droplet on the thin film can be controlled not only by varying the length of the alkyl chain for alkylamines but also by ultraviolet irradiation while maintaining superhydrophobic surfaces.

Finally, the contact angle was also measured for the other titanium phosphate thin films: the nanobelt (Figure 1a), microflower (Figure 3b), nanoplate (Figure 4b), and nanosheet (Figure 5a) structures. The contact angle for all four thin films was 0°. Therefore, all of the titanium phosphate thin films presented in this study exhibit superhydrophilic properties. This should allow excellent biocompatibility between the titanium phosphate thin films and body fluids or blood. Therefore, the micro- and nanostructured titanium phosphate thin films are assumed to be useful as implant materials. On the other hand, the contact angles of the nanobelt, microflower, nanoplate, and nanosheet thin films treated with the *n*-dodecylamine hydrochloride solution were 25°, 98°, 151°, and 128°, respectively, as shown in Figure S7 in the Supporting Information. The surface topography and composition of thin films also play a crucial role in their wettability. The surface topography can be mainly explained by the surface waviness and roughness. The nanorod thin films have a flat surface with hardly any waviness when examined at a scale of tens of micrometers, as shown in Figure 5d; however, the surface is very rough due to the nanorods and the spaces between them, and it has a fine uniform structure, as shown in Figure 5e. The distance between the convex parts is short, and the number of convex parts per unit area is large; however, the area of each convex part is small. These features of surface topography can lead to the superhydrophobicity. However, the nanobelt itself in the nanobelt thin film is soft and deformable where the ratio of the concave area to the convex area at the nanobelt tip is greater (see Figures 1a and 1b) and the distance between the convex areas is long, while the concave areas are large, resulting in the significantly smaller contact angle than that of the nanorod thin film. In the microflower thin film, surface waviness is found between flowerlike structures at a scale of tens of micrometers, where the long thin plate that forms the flowerlike structure and the surface roughness in between the plates are large, but the contact angle is smaller compared to that of the nanorod thin film due to areas not covered by the flowerlike structure (Figure 3b) and areas in which flowerlike structures are broken (Figure 3e). The nanoplate thin film has the large contact angle similar to that of the nanorod thin film due to the surface waviness between the hemispherical nanoplate aggregates shown in Figure 4b and surface roughness created by the aggregation of nanoplates, as shown in Figure 4c. The nanosheet thin film has a surface waviness (unevenness at the scale of a few micrometers) as a result of aggregated nanosheets shown in Figure 5b, but it has a slightly smaller contact angle than that of the nanorod thin film because of the smaller surface roughness than that of the nanorod thin film.

## 4. CONCLUSIONS

In the present study, hydrothermal treatment of a titanium plate in a mixed aqueous hydrogen peroxide and aqueous phosphoric acid solution under different conditions resulted in titanium phosphate thin films possessing various crystal structures and micro- and nanoscale morphologies that have not been previously reported. The results of this study also clarify the mechanisms behind the formation of these thin films. The crystal structure and morphology of the titanium phosphate thin film depended strongly on the concentration of aqueous hydrogen peroxide solution, the amount of aqueous phosphoric acid solution, and the reaction temperature. In particular, hydrogen peroxide was found to play an important role in the formation of the titanium phosphate thin films. The titanium phosphate thin films obtained in this study had superhydrophilic properties. Superhydrophobic surfaces with controllable adhesion were obtained on $\pi$-titanium phosphate nanorod thin films modified with alkylamine molecules. The adhesion force between a water droplet and the thin film depended on the alkyl chain length of the alkylamine and the ultraviolet irradiation. The procedure for controlling the wettability and adhesion of thin films to water droplets by utilizing the difference in the alkyl chain length proposed in this study is much simpler than previously reported procedures. Moreover, determining the wettability of the prepared titanium phosphate thin films and films modified using organic molecules can help us in understanding the influence of micro- and nanostructures on the wettability of these films. The micro- and nanostructured titanium phosphate thin films may have a number of applications such as use as biomaterials, catalysts, and energy materials and in liquid transportation, separation of toxic substances or useful substances, oil−water separation, and decomposition of toxic organic substances.

## ■ ASSOCIATED CONTENT

### Ⓢ Supporting Information

EDX spectra, SEM images, XRD pattern,photographs taken with a digital camera, and FT-IR spectrum. This material is available free of charge via the Internet at http://pubs.acs.org.

## ■ AUTHOR INFORMATION

### Corresponding Author

*E-mail: yada@cc.saga-u.ac.jp.

### Notes

The authors declare no competing financial interest.

## ■ ACKNOWLEDGMENTS

This research was partially supported by KAKENHI (25420732) and Dean's Grant for Progressive Research Projects of Saga University.

## ■ REFERENCES

(1) Christensen, A. N.; Anderson, E. K.; Anderson, I. G.; Albrti, G.; Nielsen, M.; Lehmann, M. S. X-Ray Powder Diffraction Study of Layer Compounds. The Crystal Structure of $\alpha$-Ti$(HPO_4)_2\cdot H_2O$ and a Proposed Structure for $\gamma$-Ti$(H_2PO_4)(PO_4)\cdot 2H_2O$. *Acta Chem. Scand.* **1990**, *44*, 865−872.

(2) Bortun, A. I.; Khainakov, S. A.; Bortun, L. N.; Poojary, D. M.; Rodriguez, J.; Garcia, J. R.; Clearfield, A. Synthesis and Characterization of Two Novel Fibrous Titanium Phosphates $Ti_2O(PO_4)_2\cdot 2H_2O$. *Chem. Mater.* **1997**, *9*, 1805−1811.

(3) Poojary, D. M.; Bortun, A. I.; Bortun, L. N.; Clearfield, A. Synthesis and X-Ray Powder Structures of Three Novel Titanium Phosphate Compounds. *J. Solid State Chem.* **1997**, *132*, 213−223.

(4) Bhaumik, A.; Inagaki, S. Mesoporous Titanium Phosphate Molecular Sieves with Ion-Exchange Capacity. *J. Am. Chem. Soc.* **2001**, *123*, 691−696.

(5) Yin, Z.; Sakamoto, Y.; Yu, J.; Sun, S.; Terasaki, O.; Xu, R. Microemulsion-Based Synthesis of Titanium Phosphate Nanotubes via Amine Extraction System. *J. Am. Chem. Soc.* **2004**, *126*, 8882−8883.
(6) Peng, J.; Feng, L.-N.; Ren, Z.-J.; Jiang, L.-P.; Zhu, J.-J. Synthesis of Silver Nanoparticle-Hollow Titanium Phosphate Sphere Hybrid as a Label for Ultrasensitive Electrochemical Detection of Human Interleukin-6. *Small* **2011**, *7*, 2921−2928.
(7) Sarkar, K.; Nandi, M.; Bhaumik, A. Enhancement in Microporosity and Catalytic Activity on Grafting Silica and Organosilica Moieties in Lamellar Titanium Phosphate Framework. *Appl. Catal., A* **2008**, *343*, 55−61.
(8) Liu, J.; Wei, X.; Yu, Y.; Song, J.; Wang, X.; Li, A.; Liu, X.-W.; Deng, W.-Q. Uniform Core−Shell Titanium Phosphate Nanospheres with Orderly Open Nanopores: A Highly Active Brønsted Acid Catalyst. *Chem. Commun.* **2010**, *46*, 1670−1672.
(9) Santos-Peña, J.; Soudan, P.; Cruz-Yusta, M.; Franger, S. Increasing the Electrochemical Activity of Transition Metal Phosphates in Lithium Cells by Treatment with Intimate Carbon: The Case of Titanium Phosphate. *Electrochim. Acta* **2006**, *51*, 4841−4849.
(10) Cheng, P.; Lan, T.; Wang, W.; Wu, H.; Yang, H.; Deng, C.; Dai, X.; Guo, S. Improved Dye-Sensitized Solar Cells by Composite Ionic Liquid Electrolyte Incorporating Layered Titanium Phosphate. *Sol. Energy* **2010**, *84*, 854−859.
(11) Cheng, P.; Chen, R.; Wang, J.; Yu, J.; Lan, T.; Wang, W.; Yang, H.; Wu, H.; Deng, C. Promoting Effect of Layered Titanium Phosphate on the Electrochemical and Photovoltaic Performance of Dye-Sensitized Solar Cells. *Nanoscale Res. Lett.* **2010**, *5*, 1313−1319.
(12) Takahashi, H.; Oi, T.; Hosoe, M. Characterization of Semicrystalline Titanium(IV) Phosphates and Their Selectivity of Cations and Lithium Isotopes. *J. Mater. Chem.* **2002**, *12*, 2513−2518.
(13) Hayashi, A.; Nakayama, H.; Tsuhako, M. Intercalation of 2-Aminoethanethiol into Layered Titanium Phosphate and Its Adsorption of Heavy Metal Ions. *Bull. Chem. Soc. Jpn.* **2002**, *75*, 1991−1996.
(14) Maheria, K. C.; Chudasama, U. V. Sorptive Removal of Dyes Using Titanium Phosphate. *Ind. Eng. Chem. Res.* **2007**, *46*, 6852−6857.
(15) Kőrösi, L.; Papp, S.; Dékány, I. A Layered Titanium Phosphate $Ti_2O_3(H_2PO_4)_2{\cdot}2H_2O$ with Rectangular Morphology: Synthesis, Structure, and Cysteamine Intercalation. *Chem. Mater.* **2010**, *22*, 4356−4363.
(16) Wang, Q.; Zhong, L.; Sun, J.; Shen, J. A Facile Layer-by-Layer Adsorption and Reaction Method to the Preparation of Titanium Phosphate Ultrathin Films. *Chem. Mater.* **2005**, *17*, 3563−3569.
(17) Wang, Q.; Yu, H.; Zhong, L.; Liu, J.; Sun, J.; Shen, J. Incorporation of Silver Ions into Ultrathin Titanium Phosphate Films: In Situ Reduction to Prepare Silver Nanoparticles and Their Antibacterial Activity. *Chem. Mater.* **2006**, *18*, 1988−1994.
(18) Takei, T.; Yonesaki, Y.; Kumada, N.; Kinomura, N. Preparation of Oriented Titanium Phosphate and Tin Phosphate/Polyaniline Hybrid Films by Electrochemical Deposition. *Langmuir* **2008**, *24*, 8554−8560.
(19) Roy, P.; Berger, S.; Schmuki, P. $TiO_2$ Nanotubes: Synthesis and Applications. *Angew. Chem., Int. Ed.* **2011**, *50*, 2904−2939.
(20) Miyauchi, M.; Tokudome, H.; Toda, Y.; Kamiya, T.; Hosono, H. Electron Field Emission from $TiO_2$ Nanotube Arrays Synthesized by Hydrothermal Reaction. *Appl. Phys. Lett.* **2006**, *89*, 043114.
(21) Inoue, Y.; Uota, M.; Torikai, T.; Watari, T.; Noda, I.; Hotokebuchi, T.; Yada, M. Antibacterial Properties of Nanostructured Silver Titanate Thin Films Formed on a Titanium Plate. *J. Biomed. Mater. Res., Part A* **2010**, *92*, 1171−1180.
(22) Yada, M.; Inoue, Y.; Gyoutoku, A.; Noda, I.; Torikai, T.; Watari, T.; Hotokebuchi, T. Apatite-Forming Ability of Titanium Compound Nanotube Thin Films Formed on a Titanium Metal Plate in a Simulated Body Fluid. *Colloids Surf., B* **2010**, *80*, 116−124.
(23) Lu, J.-S. Corrosion of Titanium in Phosphoric Acid at 250 °C. *Trans. Nonferrous Met. Soc. China* **2009**, *19*, 552−556.
(24) Park, J.-W.; Jang, J.-H.; Lee, C. S.; Hanawa, T. Osteoconductivity of Hydrophilic Microstructured Titanium Implants with Phosphate Ion Chemistry. *Acta Biomater.* **2009**, *5*, 2311−2321.
(25) Zhang, X.; Shi, F.; Niu, J.; Jiang, Y.; Wang, Z. Superhydrophobic Surfaces: From Structural Control to Functional Application. *J. Mater. Chem.* **2008**, *18*, 621−633.
(26) Guo, Z.; Liu, W.; Su, B.-L. Superhydrophobic Surfaces: From Natural to Biomimetic to Functional. *J. Colloid Interface Sci.* **2011**, *353*, 335−355.
(27) Yan, Y. Y.; Gao, N.; Barthlott, W. Mimicking Natural Superhydrophobic Surfaces and Grasping the Wetting Process: A Review on Recent Progress in Preparing Superhydrophobic Surfaces. *Adv. Colloid Interface Sci.* **2011**, *169*, 80−105.
(28) Yao, X.; Song, Y.; Jiang, L. Applications of Bio-Inspired Special Wettable Surfaces. *Adv. Mater.* **2011**, *23*, 719−734.
(29) Tang, K.; Yu, J.; Zhao, Y.; Liu, Y.; Wang, X.; Xu, R. Fabrication of Super-Hydrophobic and Super-Oleophilic Boehmite Membranes from Anodic Alumina Oxide Film via a Two-Phase Thermal Approach. *J. Mater. Chem.* **2006**, *16*, 1741−1745.
(30) Tian, D.; Zhang, X.; Wang, X.; Zhai, J.; Jiang, L. Micro/Nanoscale Hierarchical Structured ZnO Mesh Film for Separation of Water and Oil. *Phys. Chem. Chem. Phys.* **2011**, *13*, 14606−14610.
(31) Wen, Q.; Di, J.; Jiang, L.; Yu, J.; Xu, R. Zeolite-Coated Mesh Film for Efficient Oil−Water Separation. *Chem. Sci.* **2013**, *4*, 591−595.
(32) Cassie, A. B. D.; Baxter, S. Wettability of Porous Surfaces. *Trans. Faraday Soc.* **1944**, *40*, 546−551.
(33) Zhao, N.; Xie, Q.; Kuang, X.; Wang, S.; Li, Y.; Lu, X.; Tan, S.; Shen, J.; Zhang, X.; Zhang, Y.; Xu, J.; Han, C. C. A Novel Ultra-Hydrophobic Surface: Statically Non-Wetting but Dynamically Non-Sliding. *Adv. Funct. Mater.* **2007**, *17*, 2739−2745.
(34) Wu, D.; Wu, S.-Z.; Chen, Q.-D.; Zhang, Y.-L.; Yao, J.; Yao, X.; Niu, L.-G.; Wang, J.-N.; Jiang, L.; Sun, H.-B. Curvature-Driven Reversible In Situ Switching Between Pinned and Roll-Down Superhydrophobic States for Water Droplet Transportation. *Adv. Mater.* **2011**, *23*, 545−549.
(35) Lai, Y.; Gao, X.; Zhuang, H.; Huang, J.; Lin, C.; Jiang, L. Designing Superhydrophobic Porous Nanostructures with Tunable Water Adhesion. *Adv. Mater.* **2009**, *21*, 3799−3803.
(36) Lai, Y.; Lin, C.; Huang, J.; Zhuang, H.; Sun, L.; Nguyen, T. Markedly Controllable Adhesion of Superhydrophobic Spongelike Nanostructure $TiO_2$ Films. *Langmuir* **2008**, *24*, 3867−3873.
(37) Liu, X.; Wu, W.; Wang, X.; Luo, Z.; Liang, Y.; Zhou, F. A Replication Strategy for Complex Micro/Nanostructures with Superhydrophobicity and Superoleophobicity and High Contrast Adhesion. *Soft Mater.* **2009**, *5*, 3097−3105.
(38) Bortun, A. I.; Bortun, L.; Clearfield, A.; Villa-García, M. A.; García, J. R.; Rodríguez, J. Synthesis and Characterization of a Novel Layered Titanium Phosphate. *J. Mater. Res.* **1996**, *11*, 2490−2498.
(39) Bereznitski, Y.; Jaroniec, M.; Bortun, A. I.; Poojary, D. M.; Clearfield, A. Surface and Structural Properties of Novel Titanium Phosphates. *J. Colloid Interface Sci.* **1997**, *191*, 442−448.
(40) Mühlebach, J.; Müller, K.; Schwarzenbach, G. Peroxo Complexes of Titanium. *Inorg. Chem.* **1970**, *11*, 2381−2390.
(41) Yada, M.; Inoue, Y.; Uota, M.; Torikai, T.; Watari, T.; Hotokebuchi, T. Plate, Wire, Mesh, Microsphere, and Microtube Composed of Sodium Titanate Nanotubes on a Titanium Metal Template. *Langmuir* **2007**, *23*, 2815−2823.
(42) Guo, Y.; Lee, N.-H.; Oh, H.-G.; Yoon, C.-R.; Park, K.-S.; Lee, H.-G.; Lee, K.-S.; Kim, S.-J. Structure-Tunable Synthesis of Titanate Nanotube Thin Films via a Simple Hydrothermal Process. *Nanotechnology* **2007**, *18*, 295608.
(43) Wu, J.-M. Low-Temperature Preparation of Titania Nanorods through Direct Oxidation of Titanium with Hydrogen Peroxide. *J. Cryst. Growth* **2004**, *269*, 347−355.
(44) Feng, L.; Zhang, Y.; Xi, J.; Zhu, Y.; Wang, N.; Xia, F.; Jiang, L. Petal Effect: A Superhydrophobic State with High Adhesive Force. *Langmuir* **2008**, *24*, 4114−4119.
(45) Uetsuka, H.; Onishi, H.; Henderson, M. A.; White, J. M. Photoinduced Redox Reaction Coupled with Limited Electron

Mobility at Metal Oxide Surface. *J. Phys. Chem. B* **2004**, *108*, 10621−10624.